

Supplementary Information

Hg₃AsS₄X (X = Cl and Br): Two Hg-based chalcogenides as long-wave infrared nonlinear optical crystals with superior comprehensive performances

Feng Xu,^{acd} Xiang Xu,^{ad} Bingxuan Li,^e Ge Zhang,^e Chan Zheng,^{*ac} Jindong Chen^{*b} and Ning Ye^{*b}

^a School of Materials Science and Engineering, Fujian University of Technology, Fuzhou 350118, China

^b Tianjin Key Laboratory of Functional Crystal Materials, Institute of Functional Crystal, Tianjin University of Technology, Tianjin 300384, China

^c Institute of Biology and Chemistry, Fujian University of Technology, Fuzhou 350118, China

^d State Key Laboratory of Structural Chemistry, Fujian Institute of Research on the Structure of Matter, Chinese Academy of Sciences, Fuzhou 350002, PR China

^e Key Laboratory of Optoelectronic Materials Chemistry and Physics, Fujian Institute of Research on the Structure of Matter, Chinese Academy of Sciences, Fuzhou, Fujian 350002, China

*Email: czheng.fjut@gmail.com, cjd1225@email.tjut.edu.cn, nye@email.tjut.edu.cn

Table of Contents

	Title	Page
Table S1	Atomic coordinates ($\times 10^4$) and equivalent isotropic displacement parameters ($\text{\AA}^2 \times 10^3$) for $\text{Hg}_3\text{AsS}_4\text{Cl}$ (HASC) and $\text{Hg}_3\text{AsS}_4\text{Br}$ (HASB)	S3
Table S2	Selected bond lengths [Å] and angles [deg] for HASC and HASB	S3
Table S3	Anisotropic displacement parameters ($\text{\AA}^2 \times 10^3$) for HASC and HASB	S4
Figure S1	Figure S1. (a) As-grown crystals for (b) HASC and (c) HASB. Polished crystal wafers for (d) HASC and (e) HASB.	S5
Figure S2	Calculated and experimental powder X-ray diffraction patterns for (a) HASC and (b) HASB	S5
Figure S3	EDS analyses for (a) HASC and (b) HASB	S6
Figure S4	Calculated refractive index dispersion curves for (a) HASC and (b) HASB	S6
Figure S5	PL decay curves for (a) HASC and (b) HASB. The power-dependent PL intensity experimental results for (c) HASC and (d) HASB. PL spectra over the temperature range of 10-300 K for (e) HASC and (f) HASB.	S7
Figure S6	TG and DTA curves for (a) HASC and (b) HASB. The PXRD patterns at various temperatures for (c) HASC and (d) HASB	S7
Figure S7	Calculated electronic band structure for (a) HASC and (b) HASB	S8
Figure S8	DOS and PDOS plots for (a) HASC and (b) HASB	S8
Figure S9	Electron density calculation for (a) HASC and (b) HASB	S8
	The Anionic Group Theory Calculation	S9

Table S1. Atomic coordinates ($\times 10^4$) and equivalent isotropic displacement parameters ($\text{\AA}^2 \times 10^3$) for $\text{Hg}_3\text{AsS}_4\text{Cl}$ (HASC) and $\text{Hg}_3\text{AsS}_4\text{Br}$ (HASB).

Atom	x	y	z	U(eq)
$\text{Hg}_3\text{AsS}_4\text{Cl}$				
Hg(1)	4959(1)	5041(1)	5109(1)	23(1)
S(1)	8517(2)	7034(4)	6246(5)	12(1)
Cl(1)	6667	3333	2905(7)	20(1)
As(1)	10000	10000	4885(2)	10(1)
S(2)	3333	6667	3708(7)	14(1)
$\text{Hg}_3\text{AsS}_4\text{Br}$				
Hg(1)	-4955(1)	-5045(1)	-4659(1)	25(1)
Br(1)	-6667	-3333	-2437(4)	20(1)
S(1)	-2983(5)	-1492(3)	-5795(5)	15(1)
As(1)	0	0	-4485(4)	13(1)
S(2)	-3333	-6667	-3289(8)	15(1)

U(eq) is defined as one third of the trace of the orthogonalized U_{ij} tensor.

Table S2. Selected bond lengths [Å] and angles [deg] for HASC and HASB.

$\text{Hg}_3\text{AsS}_4\text{Cl}$		$\text{Hg}_3\text{AsS}_4\text{Br}$	
Hg(1)-S(1)	2.519(2)	Hg(1)-S(1)	2.527(3)
Hg(1)-S(2)	2.449(3)	Hg(1)-S(2)	2.450(4)
Hg(1)-Cl(1)	2.968(5)	Hg(1)-Br(1)	3.029(3)
S(1)-As(1)	2.274(4)	S(1)-As(1)	2.278(5)
S(1)-Hg(1)-S(1)#1	110.32(17)	S(1)-Hg(1)-Br(1)	89.70(8)
S(1)-Hg(1)-Cl(1)	88.58(7)	S(1)#1-Hg(1)-Br(1)	89.70(8)
S(2)-Hg(1)-S(1)	123.60(6)	S(1)#1-Hg(1)-S(1)	108.77(19)
S(2)-Hg(1)-Cl(1)	106.9(2)	S(2)-Hg(1)-Br(1)	105.20(19)
Hg(1)-S(1)-Hg(1)#2	98.48(13)	S(2)-Hg(1)-S(1)	124.29(8)
As(1)-S(1)-Hg(1)	102.11(14)	Hg(1)#1-Br(1)-Hg(1)#2	78.15(9)

Hg(1)#2-Cl(1)-Hg(1)	80.02(15)	Hg(1)#2-S(1)-Hg(1)	98.15(15)
S(1)-As(1)-S(1)#3	93.59(16)	As(1)-S(1)-Hg(1)	101.41(17)
S(1)-As(1)-S(1)#4	93.59(16)	S(1)#3-As(1)-S(1)#4	93.8(2)
Hg(1)#5-S(2)-Hg(1)#6	95.76(18)	Hg(1)#5-S(2)-Hg(1)#6	95.2(2)

Symmetry transformations used to generate equivalent atoms:

#1 -y+1,x-y,z #2 -x+y+1,-x+1,z #3 -x+y+1,-x+2,z

#4 -y+2,x-y+1,z #5 -y+1,x-y+1,z #6 -x+y,-x+1,z

Table S3. Anisotropic displacement parameters ($\text{\AA}^2 \times 10^3$) for HASC and HASB.

The anisotropic displacement factor exponent takes the form: $-2\pi^2[h^2a^*U11 + \dots + 2hka^*b^*U12]$

Atom	U11	U22	U33	U23	U13	U12
Hg ₃ AsS ₄ Cl						
Hg(1)	17(1)	17(1)	35(1)	3(1)	-3(1)	10(1)
S(1)	12(1)	9(1)	16(2)	1(1)	1(1)	4(1)
Cl(1)	24(2)	24(2)	12(3)	0	0	12(1)
As(1)	11(1)	11(1)	9(2)	0	0	6(1)
S(2)	15(2)	15(2)	10(3)	0	0	8(1)
Hg ₃ AsS ₄ Br						
Hg(1)	21(1)	21(1)	34(1)	2(1)	-2(1)	12(1)
Br(1)	25(1)	25(1)	9(1)	0	0	12(1)
S(1)	12(2)	15(1)	16(2)	1(1)	1(1)	6(1)
As(1)	15(1)	15(1)	8(2)	0	0	7(1)
S(2)	17(2)	17(2)	11(3)	0	0	8(1)

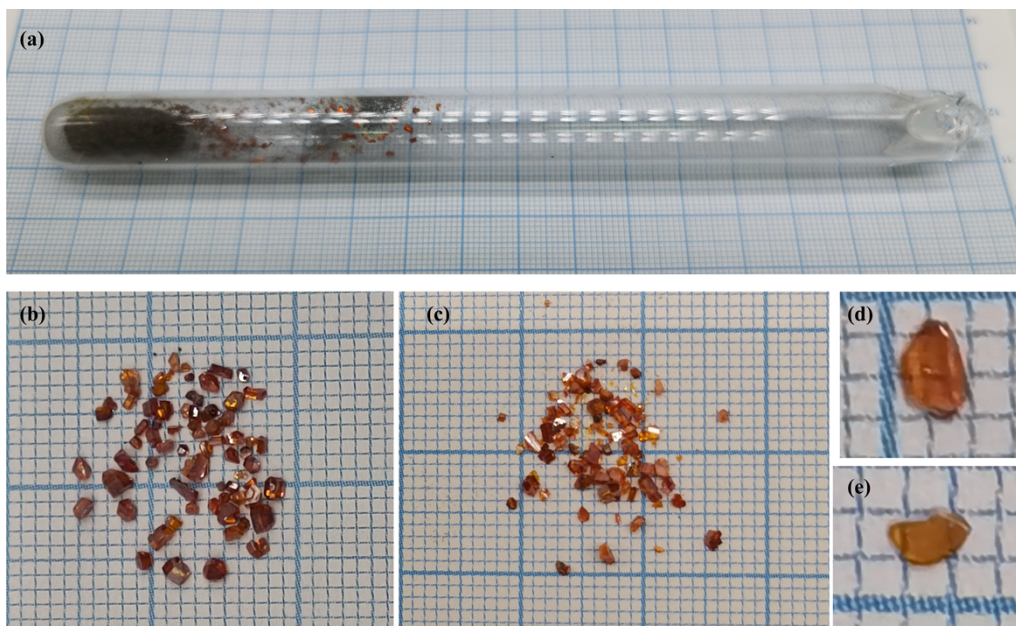


Figure S1. (a) As-grown crystals for (b) HASC and (c) HASB. Polished crystal wafers for (d) HASC and (e) HASB.

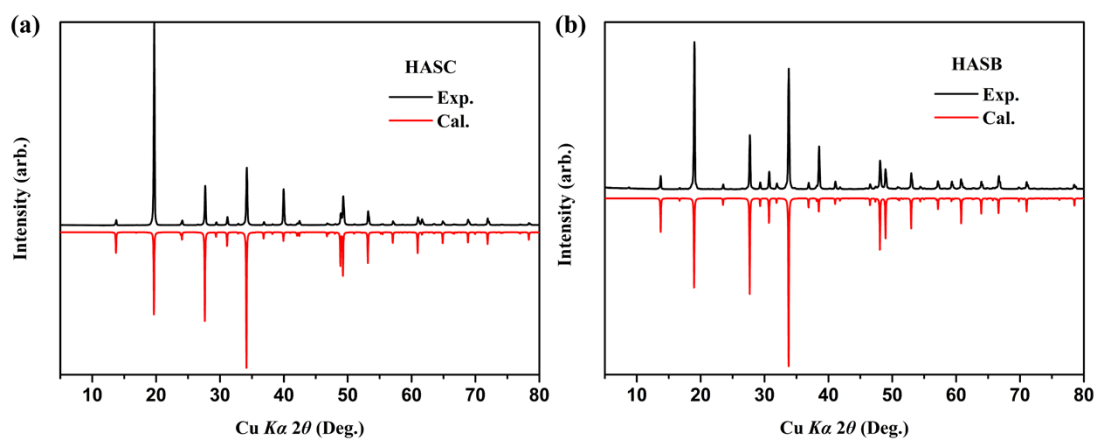


Figure S2. Calculated and experimental powder X-ray diffraction patterns for (a) HASC and (b) HASB.

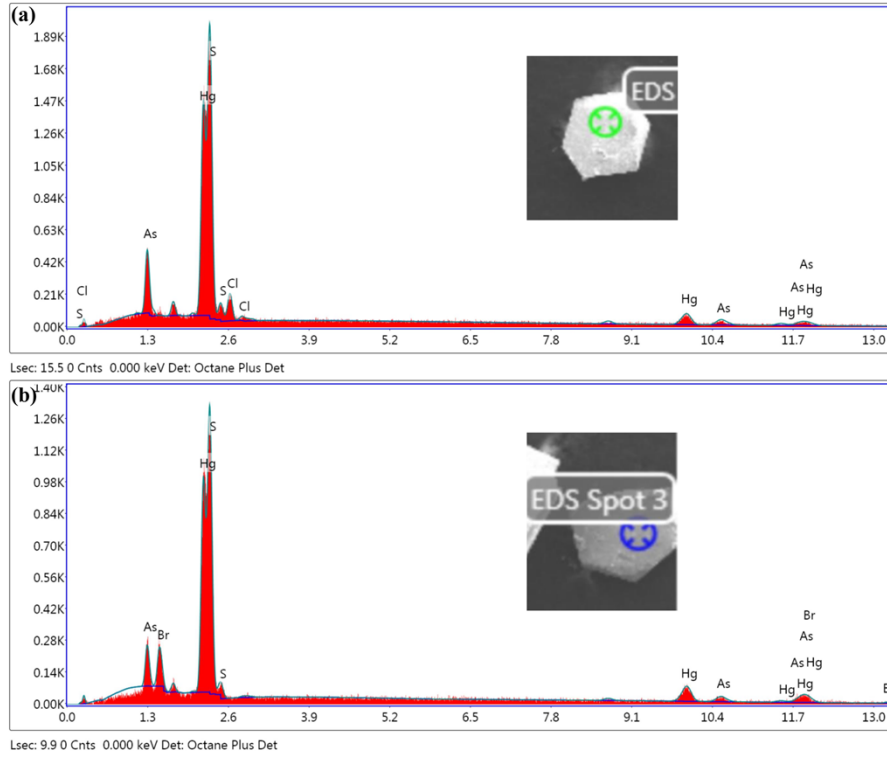


Figure S3. EDS analyses for (a) HASC and (b) HASB.

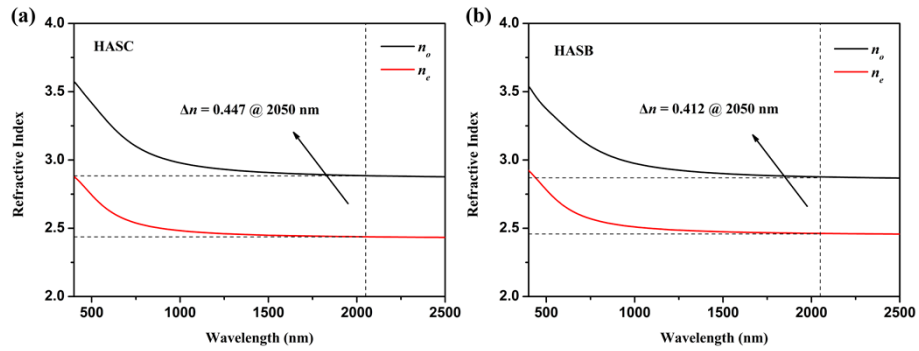


Figure S4. Calculated refractive index dispersion curves for (a) HASC and (b) HASB.

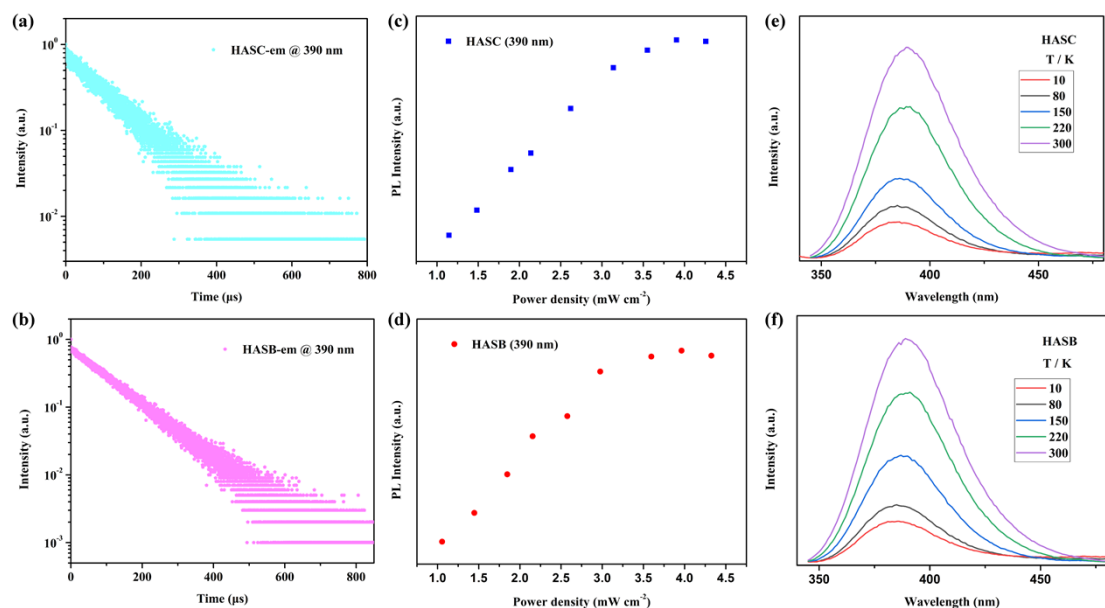


Figure S5. PL decay curves for (a) HASC and (b) HASB. The power-dependent PL intensity experimental results for (c) HASC and (d) HASB. PL spectra over the temperature range of 10–300 K for (e) HASC and (f) HASB.

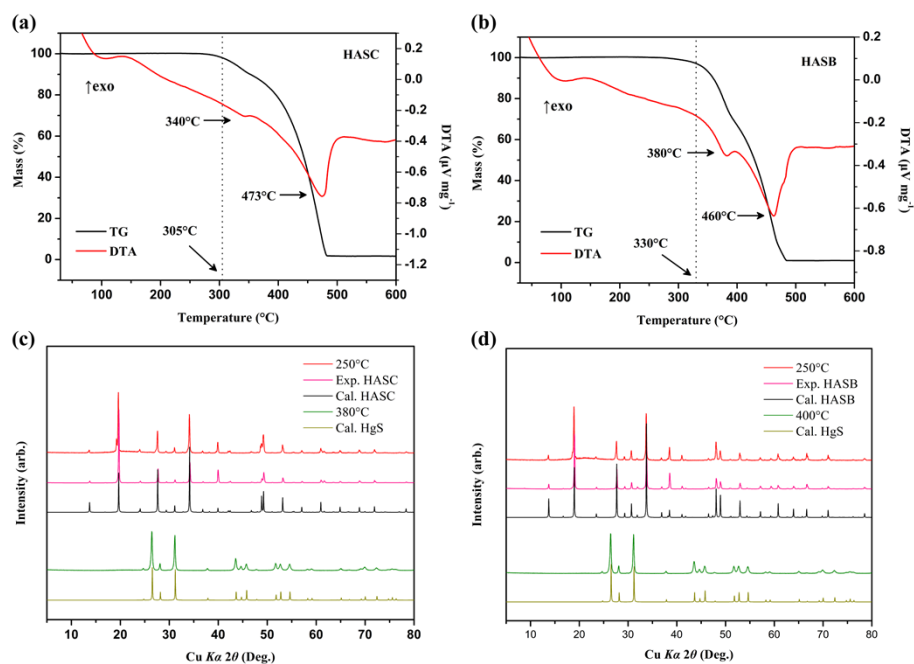


Figure S6. TG and DTA curves for (a) HASC and (b) HASB. The PXRD patterns at various temperatures for (c) HASC and (d) HASB.

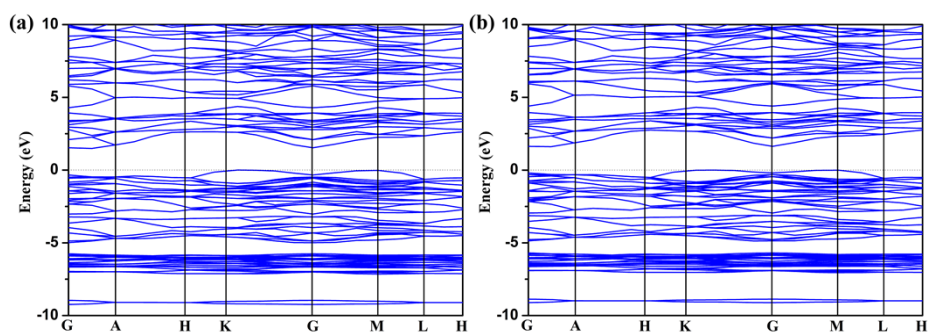


Figure S7. Calculated electronic band structure for (a) HASC and (b) HASB.

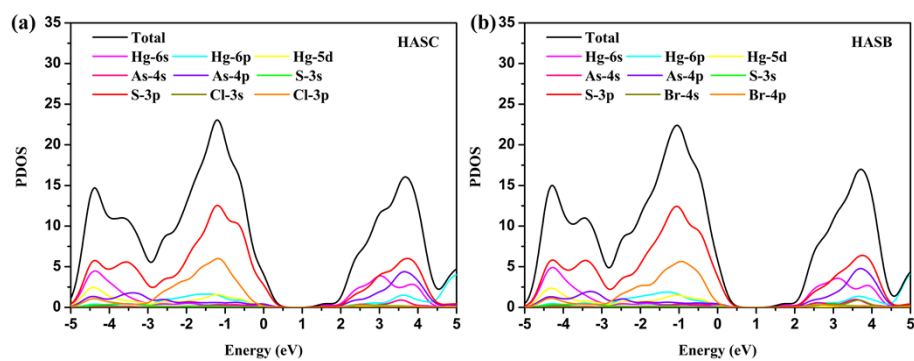


Figure S8. DOS and PDOS plots for (a) HASC and (b) HASB.

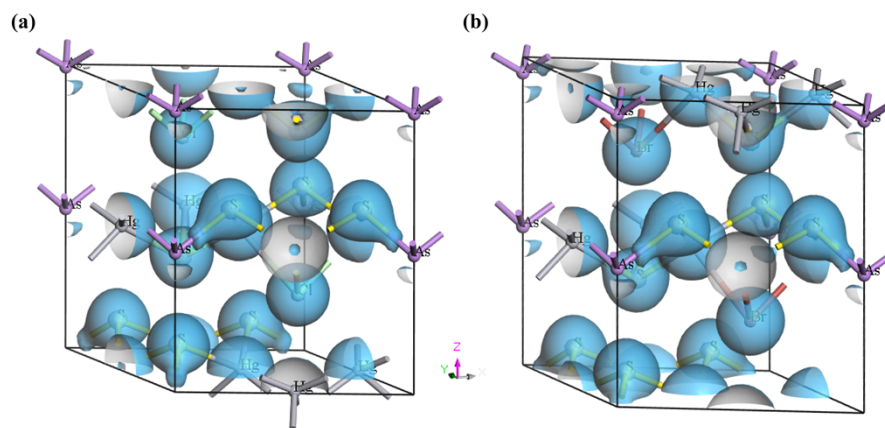


Figure S9. Electron density calculation for (a) HASC and (b) HASB.

The Anionic Group Theory Calculation

The macroscopic second-order susceptibility $\chi^{(2)}$ can be expressed as

$$\chi_{ijk}^{(2)} = \frac{F}{V} \sum_P \sum_{i'j'k'} \alpha_{ii'} \alpha_{jj'} \alpha_{kk'} \beta_{i'j'k'}^{(2)}(P), P = \text{unit} \quad (\text{S1})$$

In this expression, F denotes the correction factor of localized field, V presents the volume of the unit cell, $\alpha_{ii'}$, $\alpha_{jj'}$, and $\alpha_{kk'}$ denote the direction cosines between the macroscopic coordinate axes of the crystal and the microscopic coordinate axes groups, and $\beta_{i'j'k'}$ shows the microscopic second-order susceptibility tensors of each group.

(1) For HASC and HASB, the $[\text{HgS}_3]$ groups planar group in point group D_{3h} , which has two nonvanishing second-order susceptibilities, $\beta_{111}^{(2)} = -\beta_{122}^{(2)}$, according to the Kleinman approximation. The geometrical factor, g , can be derived as

$$\chi_{ijk}^{(2)} = \frac{F}{V} \cdot g_{ijk} \cdot \beta_{111}^{(2)}; (i, j, k = 1, 2, 3) \quad (\text{S2})$$

$$g_{ijk} = \sum_P^n [\alpha(i1)\alpha(j1)\alpha(k1) - \alpha(i1)\alpha(j2)\alpha(k2) - \alpha(i2)\alpha(j1)\alpha(k2) - \alpha(i2)\alpha(j2)\alpha(k1)] \quad (\text{S3})$$

$$g = \max(g_{ijk}) \quad (\text{S4})$$

(2) For HASC and HASB, the $[\text{AsS}_3]$ groups are aberrant tetrahedrons with point group C_{4v} , which has two nonvanishing second-order susceptibilities, $\beta_{311}^{(2)}$ and $\beta_{333}^{(2)}$ according to the Kleinman approximation. Hence, the macroscopic second-order susceptibility, derived from the geometrical factor g , can be exhibited as

$$\chi_{ijk}^{(2)} = \frac{F}{V} \cdot (g'_{ijk} \cdot \beta_{311}^{(2)} + g''_{ijk} \cdot \beta_{333}^{(2)}); (i, j, k = 1, 2, 3) \quad (\text{S5})$$

$$g'_{ijk} = \sum_P^n 2 \cdot [\alpha(i3)\alpha(j1)\alpha(k1) + \alpha(i1)\alpha(j3)\alpha(k1) + \alpha(i1)\alpha(j1)\alpha(k3)] \quad (\text{S6})$$

$$g''_{ijk} = \sum_P^n [\alpha(i3)\alpha(j3)\alpha(k3)] \quad (\text{S7})$$

Here, the geometrical factor g can be derived from g'_{ijk} and g''_{ijk} according to the relationship between the two microscopic second-order susceptibility and the establishment of microscopic coordinate system for $[\text{AsS}_3]$ groups, which is based on the symmetry. The geometrical factor, g , can be derived as

$$g = \max(g_{ijk}) \quad (\text{S8})$$

Finally, in the case of unspontaneous polarization, the structural criterion C is defined as

$$C = \frac{g}{n} \quad (\text{S9})$$

Here, n denotes the number of anionic groups in a unit cell. Generally, the correction factor of localized field F is considered to be equal because of similar refractive indices. Therefore, the NLO coefficient is proportional to density of the group (n/V), the structural criterion (C), and microscopic second-order susceptibility tensors based on the above derivation.